Improved Harmonic Current Injection Control Strategy for DC-Biased-VRM Based on Current Orthogonal Component Distribution to Enhance Output Torque

Xiang Zhang, Jiwen Zhao, *Senior Member, IEEE*, Zixiang Yu, *Member, IEEE*, and Zhenbao Pan, *Member, IEEE*

***Abstract*—This article proposes an improved harmonic current injection control strategy for dc-biased Vernier reluctance machine based on current orthogonal component distribution to enhance output torque, thereby improving the output efficiency of the machine. The effect of the interaction between the harmonic current and the inductance on average torque of the machine is analyzed. Then, a current distribution ratio with the maximum torque/current ratio is given, which can effectively increase the output torque of the machine. Based on this current ratio, a novel distribution method of harmonic current orthogonal component is proposed to provide reference value of harmonic current injection. Furthermore, in order to realize the precise injection control of amplitude and angle of harmonic current, a harmonic current orthogonal component tracking strategy with advanced angle compensation is proposed. The improved harmonic current injection control strategy presents advantages of high current control accuracy and wide applicable speed range. In addition, the parameter design of the method is relatively simple. Finally, the conclusion is verified by experiments.**

***Index Terms*—Current control, dc-biased Vernier reluctance machine (dc-biased-VRM), harmonic injection, orthogonal component distribution, torque enhancement.**

I. Introduction

THE interior of the aero-engine is a harsh environment with high speed and strong vibration, so it requires the aero-starting engine to have good adaptability in the harsh environment, excellent speed regulation performance, and simple power generation control. Among the relevant topics, the switched reluctance machine (SRM) has received extensive attention due to its simple structure and reliable operation. However, the machine presents problems of large torque ripple and difficulties of suppressing vibration noise. In addition, the power generation operation requires a large volume of filter, which limits its wide application [1].

In view of the above improvement requirements, several scholars have designed a reliable dc-biased Vernier reluctance machine (dc-biased-VRM) [2], [3], which is suitable for high-temperature and high-speed environments, especially in the field of internal starter/generator. The machine has a set of concentrated windings, which is combined with an open-winding inverter to ensure that the armature winding has dc and ac currents. The dc current regulates the excitation magnetic field, and the ac current establishes the armature magnetic field. The biased sinusoidal current helps to reduce the machine vibration noise and to enable good speed regulation performance [4], [5], [6], [7], [8]. The application of open-winding inverter also brings more possibilities for fault-tolerant control [9].

However, it is of great significance to improve the power density of the machine without using permanent magnet material. Therefore, some scholars have analyzed the mechanism of torque enhancement and proposed several machines with novel topologies that have higher torque and power density [10], [11], [12]. However, research on the control strategy can further improve the torque and power density based on the optimization of the machine body, so that the machine can adapt to more conditions. Previous literature [13] improved the average torque of SRM with several different winding configurations by injecting harmonic current. In addition, the average torque of reluctance machine was studied in [14], revealing that the second harmonic current has a greater increase to the average torque than the fourth and fifth harmonic currents. In addition, the third harmonic current will introduce torque ripple, resulting in additional copper loss and makes no contribution to the average torque [15]. Therefore, the precise control of the second harmonic current is of great significance.

In controlling the harmonic current, scholars commonly use proportional integral (PI) or proportional integral resonant (PIR) regulator. In [16], the PI regulator is used to achieve the injection of the third harmonic current under fault tolerance control, and

Manuscript received 2 January 2024; revised 19 April 2024; accepted 3 June 2024. Date of publication 11 June 2024; date of current version 4 September 2024. This work was supported in part by the National Natural Science Foundation of China Under Project 52207044 and U23A20644, and in part by the Fundamental Research Funds for the Central Universities under Grant JZ2024HGTB0227. Recommended for publication by Associate Editor R. Kennel. *(Corresponding author: Zixiang Yu.)*

The authors are with the School of Electrical Engineering and Automation, Hefei University of Technology, Hefei 230009, China (e-mail: xiangzhang@mail.hfut.edu.cn; ustczjw@hfut.edu.cn; zixiangyu@hfut.edu.cn; pzhenbao@hfut.edu.cn).

Color versions of one or more figures in this article are available at https://doi.org/10.1109/TPEL.2024.3412438.

Digital Object Identifier 10.1109/TPEL.2024.3412438

the torque ripple of the five-phase permanent magnet machine is reduced. However, PI regulator has poor effect on ac signal adjustment. As the machine speed increases, the harmonic control accuracy may further decline, and thus cannot be used in cases of high-speed requirements. In [17], multiple synchronous reference frames are introduced into the control loop, and the harmonic current is adjusted with the PI regulator. However, this approach takes up much calculation time and reduces the dynamic performance of the strategy. In [18] and [19], PIR controller is used to inject harmonic current, and the machine motion noise is successfully reduced. However, it is difficult to adjust the parameters of the controller. In [20], a generalized predictive control strategy is used to track the phase and amplitude of the harmonic current of a dual-three-phase permanent magnet synchronous machine with high precision. Adaptive notch filter (ANF) is widely used in power system, it can accurately extract the sine and cosine components of the harmonics, and the time delay is much smaller than that of the low-pass filter [21], [22]. In [23] and [24], the ANF is used to suppress the harmonics of the machine, which achieved highly accurate results and improved the speed regulation performance. Yet no research has focused on multi-harmonic active injection. Therefore, considering the above-mentioned problems in the control strategy, an improved harmonic current injection control strategy based on current orthogonal component distribution is proposed.

The main contributions of this article can be summarized as follows.

1) The increase of the average torque caused by second harmonic current is analyzed, and the relationship between the amplitude of the zero-sequence current, the fundamental current, the second harmonic current and the initial phase angle at the maximum average torque is calculated.
2) Based on the above analysis, a harmonic current orthogonal component distribution strategy is proposed to provide injection reference values for the fundamental and second harmonic currents.
3) A tracking strategy of harmonic current orthogonal component with advance angle compensation is proposed. The tracking strategy of harmonic current orthogonal component realizes the accurate control of the amplitude of harmonic current; the advance angle compensation improves the accuracy of the angle of the harmonic current injection and the stability of the control system.

The harmonic current injection control strategy proposed in this article has the following advantages.

1) The amplitude and angle of the injected harmonic current are accurately controlled, and the harmonic voltage is accurately compensated. This means that the strategy can accurately inject harmonic current, and the whole control process is clear and simple.
2) In the whole control strategy, only PI parameters and ANF iterative step need to be adjusted, so the parameter design is relatively simple.

The rest of this article is organized as follows. Section II describes the structure and principle of dc-biased-VRM. Section III discusses the effects of the second harmonic current and inductance on the average torque, and then the relationship between the amplitude and phase of the second harmonic current, the fundamental current and the dc current at the maximum torque/current ratio is given, which is used as the current distribution criterion for harmonic injection. In Section IV, a distribution method of harmonic current is proposed to provide the harmonic current orthogonal component reference value, and a tracking strategy of harmonic current orthogonal component with advance angle compensation is proposed, while accurately controlling the amplitude of the harmonic current, the accuracy of the harmonic current angle control is improved and the stability of the system is guaranteed. In Section V, experimental verification shows that this method can achieve accurate second harmonic current injection, and has a wide range of applicable speeds. Finally, Section VI concludes this article.

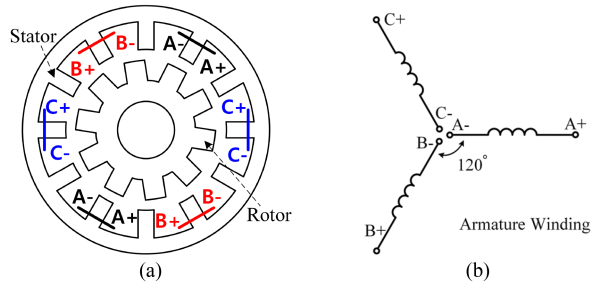

Fig. 1. DC-biased-VRM. (a) Topology. (b) Winding connection.

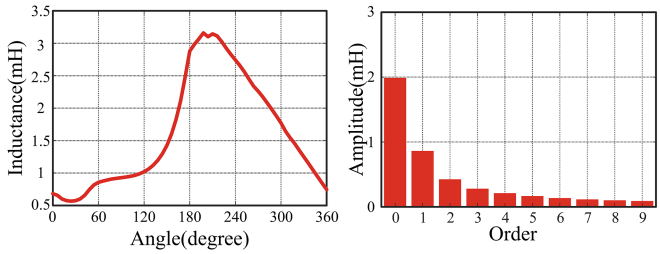

Fig. 2. Inductance waveform and FFT analysis of dc-biased-VRM under the second harmonic current injection control strategy.

II. Structure and Principle of DC-Biased-VRM

Fig. 1(a) and (b) shows the topology and winding connection of dc-biased-VRM with an open-winding structure of 12-stator 10-rotor, respectively. The machine uses a double salient pole structure, and the stator is arranged with a centralized armature winding. The open winding neutral point provides a path for zero-sequence current. The current formula of the machine can be expressed as

$$\begin{cases} I_a = I_0 + I_1 \cos(\theta_e + \alpha_1) \\ I_b = I_0 + I_1 \cos(\theta_e + \alpha_1 - 2/3\pi) \\ I_c = I_0 + I_1 \cos(\theta_e + \alpha_1 + 2/3\pi) \end{cases} \tag{1}$$

where I_0 is the amplitude of dc current, θ_e is the electrical angle, and α_1 is the initial phase angle.

Given that this machine has a concentrated winding structure, the phase inductance is mainly generated by self-inductance,

which can be expressed as

$$\begin{cases} L_a = L_0 + \sum_{j=1}^{\infty} L_j \cos(j\theta_e + \eta_j) \\ L_b = L_0 + \sum_{j=1}^{\infty} L_j \cos(j(\theta_e - 2/3\pi) + \eta_j) \\ L_c = L_0 + \sum_{j=1}^{\infty} L_j \cos(j(\theta_e + 2/3\pi) + \eta_j) \end{cases} \tag{2}$$

where L_0 is the static component of self-inductance. L_j and η_j is the amplitude and initial phase angle of the jth inductance.

The inductance of dc-biased-VRM consists mainly of components under the second-order, but the higher order components is smaller. Therefore, without considering the higher order self-inductance components and mutual inductance, the formula can be given as

$$\begin{cases} L_a = L_0 + L_1 \cos(\theta_e + \alpha_1) \\ L_b = L_0 + L_1 \cos(\theta_e + \alpha_1 - 2/3\pi) \\ L_c = L_0 + L_1 \cos(\theta_e + \alpha_1 + 2/3\pi) \end{cases}. \tag{3}$$

The voltage mathematical model can be expressed as

$$\begin{bmatrix} u_a \\ u_b \\ u_c \end{bmatrix} = R_s \begin{bmatrix} i_a \\ i_b \\ i_c \end{bmatrix} + \frac{d}{dt} \begin{bmatrix} i_a(L_0 + L_1 \cos(\theta_e)) \\ i_b(L_0 + L_1 \cos(\theta_e - 2\pi/3)) \\ i_c(L_0 + L_1 \cos(\theta_e + 2\pi/3)) \end{bmatrix}. \tag{4}$$

Using the coordinate transformation for (4), the mathematical equation in the synchronous rotating coordinate system can be obtained as (5) shown at the bottom of this page.

III. Optimal Current Configuration for Increasing Average Torque

In order to provide a reference for the injected harmonic current to effectively improve the output torque of the machine, it is necessary to analyze the distribution criterion of harmonic current when the machine torque/current ratio is maximum by combining the average torque formula.

The average torque of SRM can be expressed as

$$T_{avg} = \frac{1}{2\pi} \int_0^{2\pi} \left[\frac{P_n}{2} (i_a^2 \frac{dL_a}{d\theta_e} + i_b^2 \frac{dL_b}{d\theta_e} + i_c^2 \frac{dL_c}{d\theta_e}) \right] d\theta_e. \tag{6}$$

The three-phase current is changed to the form containing the second harmonic current as in (7), and the appropriate current amplitude and initial phase angle can enhance the average torque of the machine

$$\begin{cases} i_a = I_0 + I_1 \cos(\theta_e + \alpha_1) + I_2 \cos(2\theta_e + \alpha_2) \\ i_b = I_0 + I_1 \cos(\theta_e + \alpha_1 - 2/3\pi) \\ \quad\quad + I_2 \cos(2\theta_e + \alpha_2 + 2/3\pi) \\ i_c = I_0 + I_1 \cos(\theta_e + \alpha_1 + 2/3\pi) \\ \quad\quad + I_2 \cos(2\theta_e + \alpha_2 - 2/3\pi) \end{cases} \tag{7}$$

where I_2 and α_2 represent the amplitude and initial phase angle of the second harmonic current. By substituting (3) and (7) into (6), the formula for the average torque can be expressed as

$$\begin{aligned} T_{\text{avg\_012}} = {} & \frac{3P_n}{2} I_0 I_1 L_1 \sin(\alpha_1 - \eta_1) \\ & + \frac{3P_n}{4} I_1 I_2 L_1 \sin(-\alpha_1 + \alpha_2 - \eta_1) \end{aligned} \tag{8}$$

where $T_{\text{avg-012}}$ is the average torque of the machine. In the case specified in (9), the average torque is at maximum

$$\begin{cases} \alpha_1 - \eta_1 = \pi/2 \\ -\alpha_1 + \alpha_2 + \eta_1 = \pi/2 \end{cases}. \tag{9}$$

Assuming that the rotor teeth is aligned with one of the A-phase teeth in the initial state, then η_1 is 0, and the optimal initial phase angle is

$$\begin{cases} \alpha_1 = \pi/2 \\ \alpha_2 = \pi \end{cases}. \tag{10}$$

Therefore, (8) can be expressed as

$$T_{\text{avg\_012}} = \frac{3P_n}{2} I_0 I_1 L_1 + \frac{3P_n}{4} I_1 I_2 L_1. \tag{11}$$

In addition, to facilitate the analysis, the phase current root mean square (I_{rms}) is used to constrain the amplitude of each current

$$\sqrt{I_0^2 + I_1^2/2 + I_2^2/2} = I_{\text{rms}}. \tag{12}$$

To calculate the optimal current and phase distribution under the constraint of (12), the Lagrange multiplier method is used:

$$\begin{aligned} F(I_0, I_1, I_2, \lambda) = {} & \frac{3P_n}{2} I_0 I_1 L_1 + \frac{3P_n}{4} I_1 I_2 L_1 \\ & + \lambda(I_0^2 + I_1^2/2 + I_2^2/2 - I_{\text{rms}}^2) \end{aligned} \tag{13}$$

where λ is the Lagrange multiplier coefficient. By calculating the partial derivatives of I_0, I_1, I_2 and λ for $F(I_0, I_1, I_2, \lambda)$ and making them equal to zero, (14) can be obtained.

$$\begin{bmatrix} u_d \\ u_q \\ u_0 \end{bmatrix} = R_s \begin{bmatrix} i_d \\ i_q \\ i_0 \end{bmatrix} + \begin{bmatrix} L_0 + L_1 \cos(3\theta_e)/2 & -L_1 \sin(3\theta_e)/2 & L_1 \\ -L_1 \sin(3\theta_e)/2 & L_0 - L_1 \cos(3\theta_e)/2 & 0 \\ L_1/2 & 0 & L_0 \end{bmatrix} \begin{bmatrix} di_d/dt \\ di_q/dt \\ di_0/dt \end{bmatrix} + \omega_e \begin{bmatrix} -L_1 \sin(3\theta_e) & -L_0 - L_1 \cos(3\theta_e) & 0 \\ L_0 - L_1 \cos(3\theta_e) & L_1 \sin(3\theta_e) & L_1 \\ 0 & 0 & 0 \end{bmatrix} \begin{bmatrix} i_d \\ i_q \\ i_0 \end{bmatrix}. \tag{5}$$

From (14), the corresponding I_0, I_1, and I_2 with the highest average torque are shown as

$$\begin{cases} \frac{\partial F}{\partial I_0} = \frac{3}{2}P_n I_1 L_1 + 2\lambda I_0 = 0 \\ \frac{\partial F}{\partial I_1} = \frac{3}{2}P_n I_0 L_1 + \frac{3}{4}P_n I_2 L_1 + \lambda I_1 = 0 \\ \frac{\partial F}{\partial I_2} = \frac{3}{4}P_n I_1 L_1 + \lambda I_2 = 0 \\ \frac{\partial F}{\partial \lambda} = I_0^2 + \frac{I_1^2}{2} + \frac{I_2^2}{2} - I_{\text{rms}}^2 = 0 \end{cases} \tag{14}$$

$$\begin{cases} I_1 = I_{\text{rms}} \\ I_0 = I_2 = \frac{1}{\sqrt{3}} I_{\text{rms}} \end{cases}. \tag{15}$$

By substituting (15) into (11), the maximum average torque can be

$$\max(T_{\text{avg\_012}}) = \frac{9P_n L_1 I_{\text{rms}}^2}{4\sqrt{3}}. \tag{16}$$

Normally, dc-biased-VRM only requires dc and ac currents to work properly. In this case, the same method can be used to obtain the maximum average torque of the conventional maximum torque/current ratio control strategy, as shown in

$$\max(T_{\text{avg\_01}}) = \frac{3P_n L_1 I_{\text{rms}}^2}{2\sqrt{2}} \tag{17}$$

where $T_{\text{avg\_01}}$ is the average torque obtained by the action of dc and fundamental current.

By comparing these two different current distribution methods, it can be seen that the injection of second harmonic can increase the average torque of dc-biased-VRM by approximately 22% under the same parameters and constraints

$$\frac{\max(T_{\text{avg\_012}})}{\max(T_{\text{avg\_01}})} = \frac{\sqrt{6}}{2} \approx 1.22. \tag{18}$$

However, the second and third components of the self- inductance increase when the harmonic current of dc-biased-VRM is configured to (10) and (15). Through finite element simulation, the self-inductance waveform and fast Fourier transform (FFT) analysis at 1500 r/min and I_{rms} of 19 A are obtained, as shown in Fig. 2. The amplitude of the second and third self-inductance components are 0.27 and 0.22 mH, respectively. In this case, the role of the second and third self-inductance components cannot be ignored.

Rewrite (8) as (19). L_1 and L_2 are the second and third components of self-inductance, respectively. η_1 and η_2 are the initial phase angle of L_1 and L_2, respectively. According to (19) shown at the bottom of this page, when the effects of second and third self-inductance components on the average torque are considered, the average torque is theoretically increased by 9.21%.

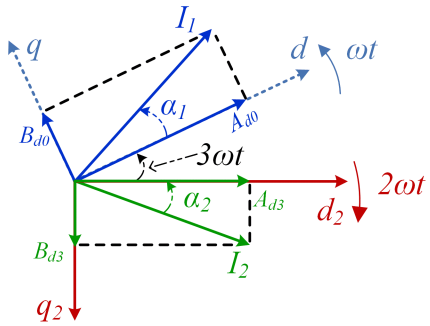

Fig. 3. Decomposition of the fundamental and second harmonic current in synchronous rotating coordinate system.

IV. Improved Harmonic Current Injection Control Strategy Based on Current Orthogonal Component Distribution

According to the analysis in Section III, the average torque and power density of the machine can be effectively improved by injecting suitable second harmonic current. In order to inject the second harmonic current accurately, the current components in the synchronous rotating coordinate system need to be accurately distributed and tracked. Therefore, the harmonic current orthogonal component distribution strategy is proposed to provide the harmonic injection reference value under the optimal distribution. Then, a current tracking strategy of harmonic current orthogonal component with advance angle compensation is proposed to achieve accurate injection of second harmonic current.

A. Novel Harmonic Current Orthogonal Component Distribution Strategy

According to Fig. 3, the $dq0$-axis current can be represented as (20). In (20), α_1 and α_2 represent the initial phase angle of the fundamental current and the second harmonic current, respectively,

$$\begin{cases} I_d = I_1\cos(\alpha_1) + I_2\cos(3\theta_e + \alpha_2) \\ I_q = I_1\sin(\alpha_1) - I_2\sin(3\theta_e + \alpha_2) \\ I_0 = I_0 \end{cases}. \tag{20}$$

The fundamental current is reflected as dc current on the dq-axis, while the second component is transformed into the third current. Furthermore, rewrite (20) as

$$\begin{cases} I_d = A_{d0} + A_{d3}\cos(3\theta_e) + B_{d3}\sin(3\theta_e) \\ I_q = A_{q0} + A_{q3}\cos(3\theta_e) + B_{q3}\sin(3\theta_e) \\ I_0 = A_{00} \end{cases} \tag{21}$$

where A_{d0}, A_{q0}, and A_{00} are the amplitude of the dc component. A_{d3}, B_{d3}, A_{q3}, and B_{q3} are the amplitude of the third harmonic

$$T'_{\text{avg\_012}} = \frac{3P_n}{2} I_0 I_1 L_1 \sin(\alpha_1 - \eta_1) + \frac{3P_n}{4} I_1 I_2 L_1 \sin(-\alpha_1 + \alpha_2 - \eta_1) + \frac{3P_n}{4} I_1^2 L_2 \sin(2\alpha_1 - \eta_2) + 3P_n I_0 I_2 L_2 \sin(\alpha_2 - \eta_2) + \frac{9P_n}{4} I_1 I_2 L_3 \sin(\alpha_1 + \alpha_2 - \eta_3). \tag{19}$$

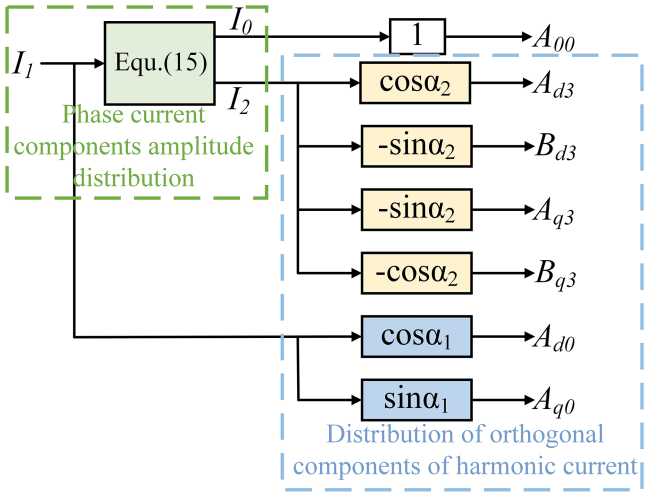

Fig. 4. Distribution method of harmonic current orthogonal component.

orthogonal component. Taking these static current components as reference value and controlling them by a specific method, the accurate injection of the second harmonic current can be realized. The proposed harmonic current orthogonal component distribution strategy is shown in Fig. 4. First, the output of the velocity loop PI regulator is adjusted to the $I_{\rm rms}$ (that is, the amplitude of the fundamental current), and then the amplitude of the zero-sequence current and the amplitude of the second harmonic current are allocated according to (15). Further, the initial phase angle of the fundamental current and the second harmonic current is adjusted by (10), and the reference value of the static current orthogonal component is allocated according to the current amplitude obtained in the previous step, which provides a basis for the control of harmonic current injection.

B. Feedback Harmonic Current Extraction Using ANF

To improve the precision of harmonic current injection, the ANF is used to detect harmonic current components on the *dq*0-axis, which can be expressed as

$$\begin{aligned} &e(n) = i(n) - f(n) \\ &f(n) = V \cdot A^T(n) \\ &A(n+1) = A(n) + \lambda e(n) V \\ &V = [1, \cos(3\theta_e), \sin(3\theta_e)] \\ &A(n) = [A_0, A_3, B_3] \\ &A(n+1) = [\hat{A}_0, \hat{A}_3, \hat{B}_3] \end{aligned} \tag{22}$$

where *i* is the feedback current signal of the machine, which contains the injected harmonic current. *f* is the extracted harmonic components, and *e* is the error signal of *i* and *f*. Moreover, ***V*** is the reference angle vector for the dc and orthogonal decomposition components of the feedback current. ***A*** is the amplitude vector of the dc and orthogonal components of the extracted feedback current. λ is the iteration step. If λ is too small, the harmonic current components will be extracted slowly and the dynamic response ability will be reduced. If λ is too large, then the extracted harmonic current components will contain more noise, resulting in lower precision of harmonic current injection. Therefore, it is necessary to adjust the iteration step size in experimental application to achieve a balance between responsiveness and noise size [23].

C. Tracking Strategy of Harmonic Current Orthogonal Component With Advance Angle Compensation

Although the conventional PI regulator has a simple structure and convenient parameter setting, tracking and adjusting the high-frequency alternating error signal remain difficult due to its limited bandwidth. Therefore, this strategy adopts ANF controller to extract the amplitude of the target signal quickly and accurately, and then uses the PI regulator to adjust.

First of all, the second harmonic current in the phase current is a third harmonic current on the *dq*-axis, thus, ANF is used to detect and extract the amplitude of the sine and cosine components of the third harmonic current in the *dq*-axis. Then, the extracted static amplitude signals are compared with the reference value respectively, and the errors are adjusted by PI regulator to get the control voltage signals.

However, dc-biased-VRM does not use permanent magnets, and thus the current regulator voltage output is applied to the stator windings, making the harmonic voltage component being 90° ahead of the corresponding harmonic current component. Therefore, the regulating voltage output of the PI regulator cannot be directly applied to the machine. In addition, the digital delay will lead to the decrease of the injection accuracy of the harmonic current angle and affect the stability of the system. Therefore, an advance phase angle compensation strategy is proposed to solve the above two problems. First, the reference value of the amplitude of components of fundamental current should be modified to (25) according to the delay angle through (23) and (24). In addition, in order to compensate the control delay of the third harmonic current on the *d*-axis and *q*-axis, $\Delta\theta_e$ is compensated to the sampled electrical angle θ_e. Second, the output of the PI regulator needs to be rotated 90° to compensate for the harmonic voltage

$$\begin{cases} I_d = I_1 \cos(\alpha_1 + \Delta\theta_e) + I_2 \cos(3\theta_e + \alpha_2) \\ I_q = I_1 \sin(\alpha_1 + \Delta\theta_e) - I_2 \sin(3\theta_e + \alpha_2) \\ I_0 = I_0 \end{cases} \tag{23}$$

$$\Delta\theta_e = \pi T_s N_r P_n / 30. \tag{24}$$

In (24), T_s is the control period, N_r is the speed of the rotor, and P_n is the number of poles of the machine

$$\begin{cases} I_d = A_{rd0} + A_{rd3} \cos(3\theta_e) + B_{rd3} \sin(3\theta_e) \\ I_q = A_{rq0} + A_{rq3} \cos(3\theta_e) + B_{rq3} \sin(3\theta_e) \\ I_0 = A_{r00} \end{cases}. \tag{25}$$

In (25), A_{rd0}, A_{rq0}, and A_{00} are the amplitude of the dc components. A_{rd3}, B_{rd3}, A_{rq3}, and B_{rq3} are the amplitude of the third harmonic components.

Fig. 5 shows the tracking strategy of harmonic current orthogonal component with advance angle compensation for the *q*-axis. In Fig. 5, i_{rq3} and u_{q3} represent the reference third harmonic current vector and the third harmonic voltage vector at the sampling time, respectively. u'_{q3} represents the third harmonic voltage when the compensation voltage is applied, and u_{q31} and u_{q32} are the cosine and sine components of u'_{q3}, respectively.

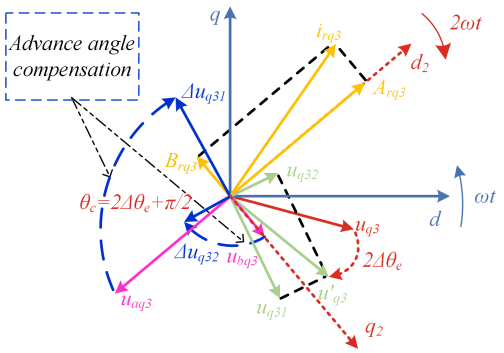

Fig. 5. Tracking strategy of harmonic current orthogonal component on q-axis.

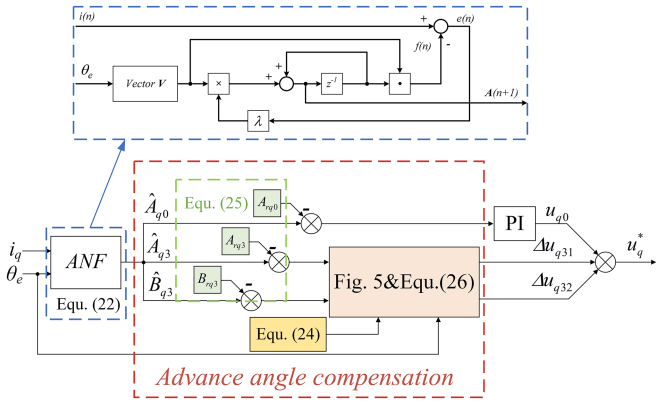

Fig. 6. Q-axis harmonic current injector block diagram.

The angle of u'_{q3} leading u_{q3} in phase is $2\Delta\theta_e$. In order to realize the accurate injection of harmonic current, it is necessary to compensate the harmonic voltage completely. Therefore, u'_{q3} needs to be completely compensated, which means that u_{q31} and u_{q32} need to be orthogonally compensated. The compensation voltage components on the q-axis are expressed as u_{aq3} and u_{bq3}. In order to orthogonally compensate u_{q31} and u_{q32}, it is necessary to advance the phase angle of u_{aq3} and u_{bq3} by θ_c, and then obtain Δu_{q31} and Δu_{q32}. By applying Δu_{q31} and Δu_{q32} to the machine, the complete compensation of harmonic voltage can be realized, and then the accurate injection of harmonic current on the q-axis can be realized.

Fig. 6 shows the structure of proposed harmonic injection control strategy on q-axis. First, ANF is used to extract the amplitude of the static component of the fundamental current and the orthogonal component of the second harmonic current in the q-axis, and they are taken as feedback values. The reference value of harmonic current injection control is provided by (25). For the static component error of the q-axis, the PI regulator is used directly to adjust it. For the error of the amplitude of the orthogonal component of the q-axis, according to (24) and (26), the compensation voltage of the PI regulator is phase-shifted, so that the second harmonic voltage can be accurately compensated and the second harmonic current can be accurately injected in phase and amplitude.

Finally, the compensation voltage of dq-axis can be obtained by (26) shown at the bottom of the next page, and the total compensation voltage can be expressed as (27). The tracking strategy of harmonic current orthogonal component with advance angle compensation proposed in this article can completely compensate the harmonic voltage, reduce the phase error of harmonic current injection, and improve the stability of the control system.

TABLE I
PARAMETERS OF THE PROTOTYPE DC-BIASED-VRM

Parameters	Description	Value
n_s	Number of stator slot	12
n_r	Number of rotor slot	10
R_s	Phase resistance (Ω)	0.088
L_0	Static inductance component (mH)	1.72
L_1	Alternating inductance component (mH)	1.04
i_{sN}	Rated current (A)	19
T_{eN}	Rated torque (N·m)	2.55
n_N	Rated speed (r/min)	1500

$$\begin{cases} u_d^* = u_{d0} + \Delta u_{d31} + \Delta u_{d32} \\ u_q^* = u_{q0} + \Delta u_{q31} + \Delta u_{q32} \\ u_0^* = u_{00} \end{cases}. \tag{27}$$

D. Overall Control Strategy of Proposed Harmonic Current Injection

In Fig. 7, the output of PI regulator of the velocity loop is adjusted to the amplitude of the fundamental current, and then the reference values of fundamental current and second harmonic current are obtained by using the novel distribution strategy of harmonic current orthogonal component. The harmonic current injector first extracts the amplitudes of the feedback current component with ANF, and then adjusts the static current amplitude error with PI regulator. Finally, the compensated voltage is obtained by using the tracking strategy of harmonic current orthogonal component with advance angle compensation proposed in this article, and the switching signal of the inverter is modulated and applied to the machine to realize the accurate injection of the second harmonic current.

V. EXPERIMENTAL VERIFICATION

To verify the control effect of the improved harmonic current injection control strategy, experiments were carried out on dc-biased-VRM machine loading platform. The machine parameters are given in Table I. The device used in this article is shown in Fig. 8. The proposed strategy is verified in TMS302F28377D DSP. The control period of the controller is 20 KHz. The function of the multi-channel recorder MSO8204 is to display and store the current waveform of the machine. The load torque, speed and power of the machine are displayed by the acquisition instrument TR-10. The high-precision digital power meter PA310 is used to record the current, voltage, and power of the inverter side.

First, the phase currents status of the proposed strategy and the improvement of the output torque of the machine are verified at speed of 1500 r/min and $I_{\rm rms}$ of 19 A. In Fig. 9(a), the machine output torque is 2.51 N·m under the conventional control

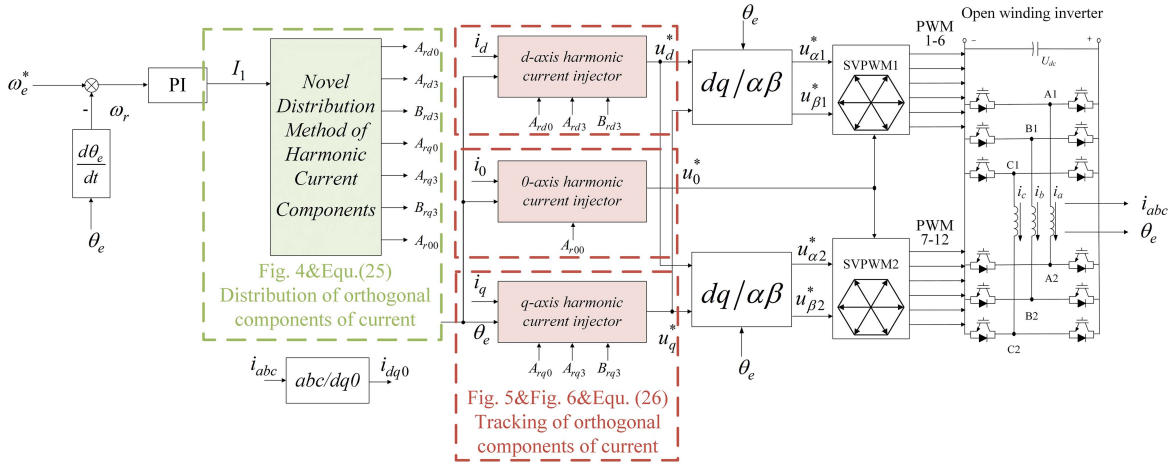

Fig. 7. Overall control strategy block diagram.

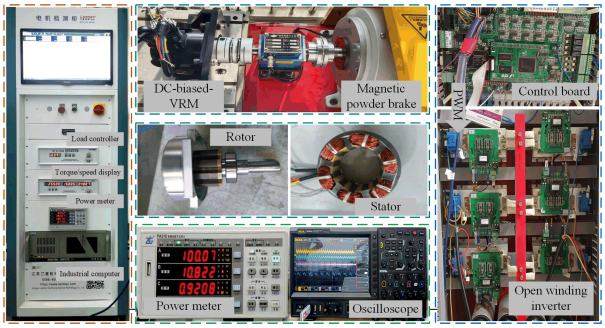

Fig. 8. Experimental equipment diagram.

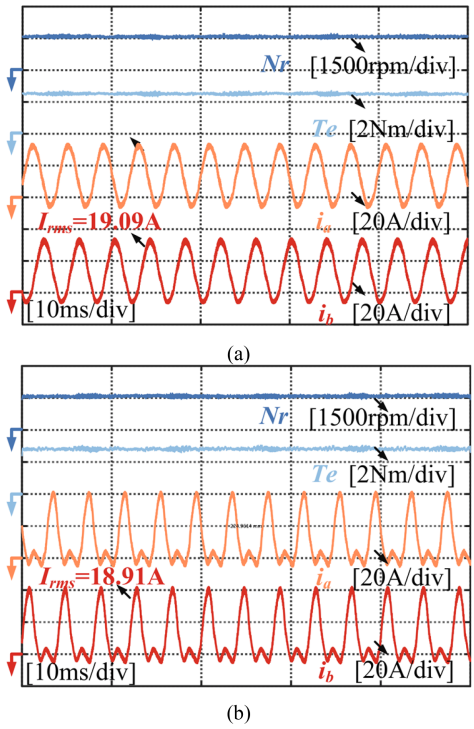

Fig. 9. The torque and current comparison of the two control strategies at 1500 r/min and $I_{\rm rms}$ of 19 A. (a) Conventional strategy. (b) Proposed strategy.

strategy. However, in Fig. 9(b), the output torque of the machine is enhanced to 2.73 N·m using the strategy proposed in this article. When the second harmonic current is actively injected into the winding, the theoretical average torque is increased by 9.21%, and the experimental average torque is increased by 8.76%. The experimental results are basically consistent with the theoretical analysis, which verifies the correctness of the theoretical analysis.

To verify that the proposed strategy can accurately control the harmonic current, experiments were conducted at 1500 r/min and $I_{\rm rms}$ of 19 A. In the experimental results, i_d, i_q, and i_0 represent the currents of d-axis, q-axis, and 0-axis, respectively. Fig. 10(a) and (b) shows the FFT analysis of the $dq0$-axis and phase currents using conventional and the proposed strategies. In Fig. 10(a), i_q and i_0 only contain the dc current. The phase current includes zero-sequence current and fundamental current. This is also proved by FFT analysis. In Fig. 10(b), i_d only contains the third harmonic current, i_q contains the dc current and the third harmonic current, and i_0 only contains the dc current. The FFT analysis results of phase current show the amplitude of each component. The zero-sequence current is 10.3 A, the fundamental current is 18.8 A, and the second harmonic current is 10.6 A, indicating that not only the zero-sequence current

$$\begin{cases} \Delta u_{d31} = [K_{pd1}(A_{rd3} - A_{d3}) + K_{id1}\int (A_{rd3} - A_{d3})dt][\cos(3\theta_e + 2\Delta\theta_e + \pi/2)] \\ \Delta u_{d32} = [K_{pd2}(B_{rd3} - B_{d3}) + K_{id2}\int (B_{rd3} - B_{d3})dt][\sin(3\theta_e + 2\Delta\theta_e + \pi/2)] \\ \Delta u_{q31} = [K_{pq1}(A_{rq3} - A_{q3}) + K_{iq1}\int (A_{rq3} - A_{q3})dt][\cos(3\theta_e + 2\Delta\theta_e + \pi/2)] \\ \Delta u_{q32} = [K_{pq2}(B_{rq3} - B_{q3}) + K_{iq2}\int (B_{rq3} - B_{q3})dt][\sin(3\theta_e + 2\Delta\theta_e + \pi/2)] \end{cases} \tag{26}$$

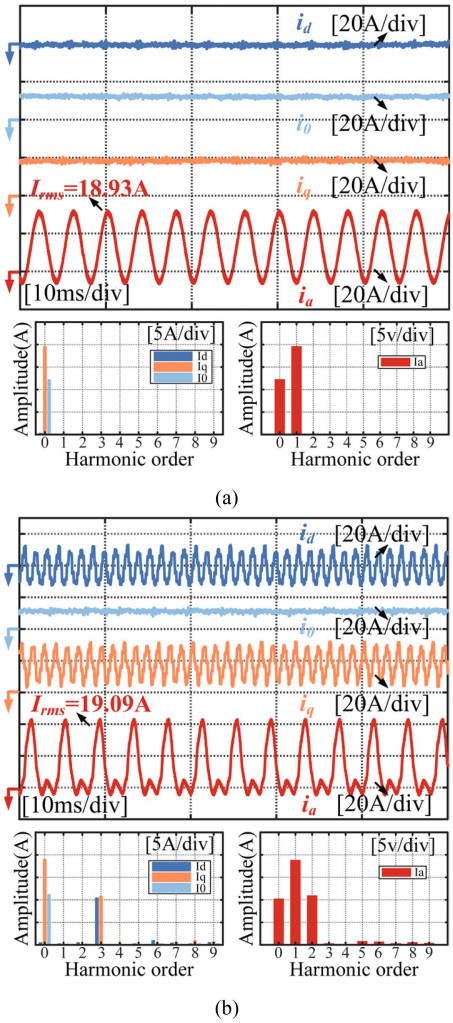

Fig. 10. Comparison of the experimental results of two control strategies at 1500 r/min and $I_{\rm rms}$ of 19 A. (a) Conventional strategy. (b) Proposed strategy.

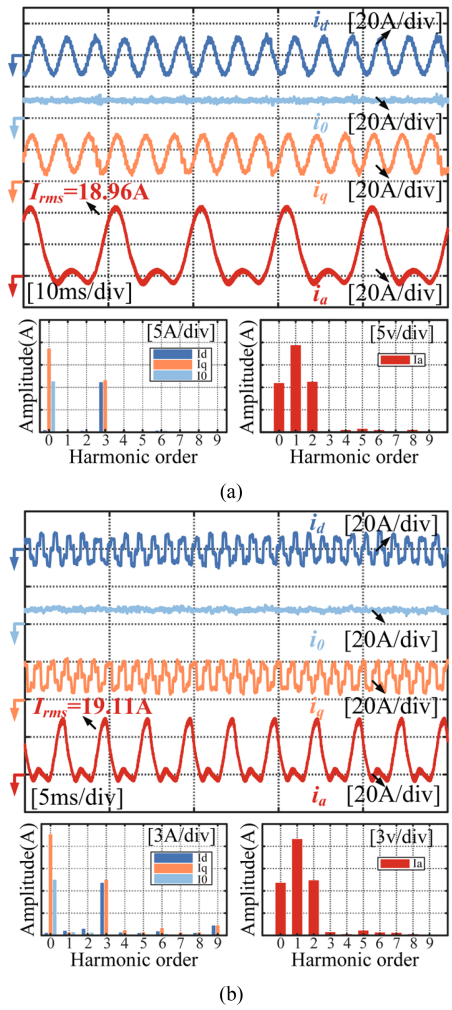

Fig. 11. Comparison of the experimental results of proposed control strategy at different speeds. (a) 600 r/min. (b) 2400 r/min.

and the fundamental current are well controlled, but the second harmonic current is also accurately controlled. Besides, a small amount of fifth and sixth harmonics can also be seen. The copper loss caused by these harmonic currents is very small, and the impact on the output efficiency of the machine is also small, so these harmonic currents can be ignored. In addition, it is worth noting that in the FFT analysis results of the *dq*-axis, the harmonics of i_d and i_q are almost third harmonics. Accurate harmonic current injection can improve the output torque of dc-biased-VRM.

Fig. 11(a) and (b) are obtained at 600 r/min and $I_{\rm rms}$ of 19 A, the speed of 2400 r/min and the machine output power of 429 W, respectively. Fig. 11(a) is the result when the machine speed is 600 r/min, and the currents of *dq*-axis are injected with the third harmonic component of the same amplitude. The FFT analysis of the phase current shows that the zero-sequence current is 10.9 A, the fundamental current is 19.3 A, and the second harmonic current is 11.2 A, which meets the proportional requirements of harmonic current distribution when the torque is maximum. Fig. 11(b) is the result when the machine speed is 2400 r/min, and the currents of *dq*-axis are also injected with the same amplitude of the third harmonic component. The FFT analysis of phase current shows that the zero-sequence current is 7.1 A, the fundamental current is 12.9 A, and the second harmonic current is 7.4 A, which also meets the requirements of harmonic current distribution when the torque is maximum. Therefore, the proposed strategy can achieve accurate injection of the second harmonic current at different speeds, ensure that the machine current accurately follows the reference value, and provide guarantee for improving the machine output torque.

In order to verify the improvement of the angle control accuracy of the harmonic current by the digital delay compensation in the advance angle compensation strategy, a comparative experiment was carried out under the condition of the machine speed of 1500 r/min and the load of 2.71 N·m. Fig. 12(a) shows the experimental result without digital delay compensation. It can be seen that there is a large angle error between the feedback current and the reference current in *dq*-axis. This angle error causes the initial phase angle of the second harmonic current to be incorrect,

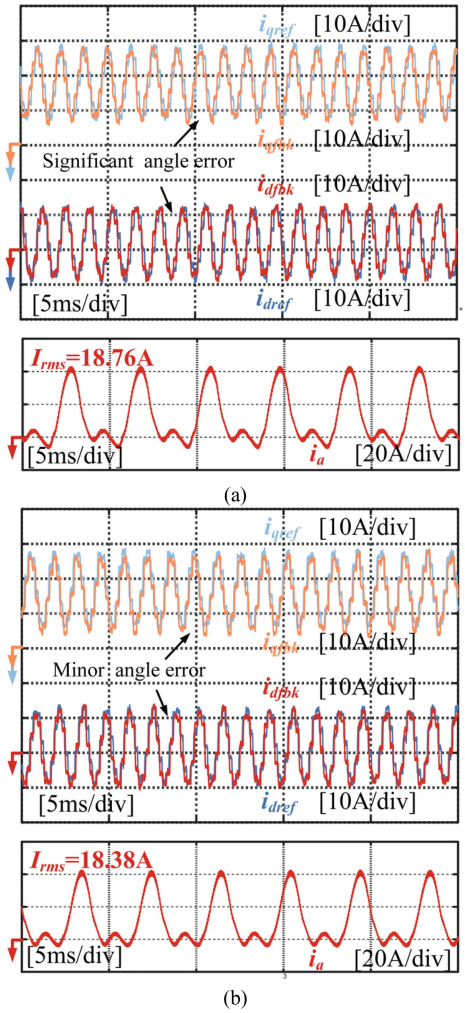

Fig. 12. Comparison of experimental results using proposed current tracking strategy when the speed is 1500 r/min and the load is 2.71 N·m. (a) Without delay compensation. (b) With delay compensation.

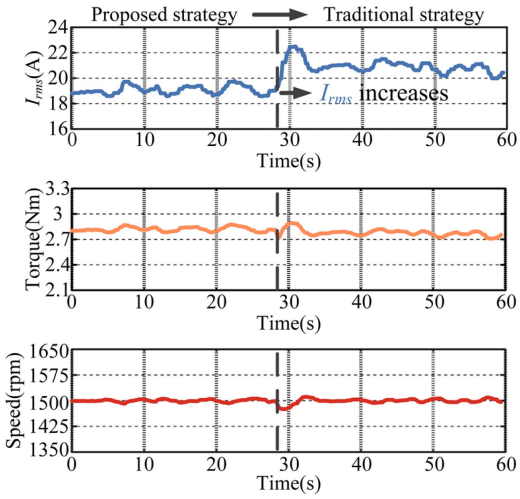

Fig. 13. Experimental results of switching from the proposed strategy to the conventional strategy under 2.76 N·m load.

which further leads to the decrease of the torque output capacity of the machine. Fig. 12(b) shows the experimental result with digital delay compensation, and the angle error between the feedback current and the reference current in dq-axis is reduced, which means that the initial phase angle of the second harmonic current in the phase current is more accurately controlled, and the smaller angle error also improves the stability of the control system. In addition, after the application of digital delay compensation, the $I_{\rm rms}$ under the same load is also reduced, which indicates that the efficiency of the machine is improved. The peak-to-peak value of the phase current is reduced from 48.4 to 46.4 A, which will reduce the impact of current fluctuations on the inverter.

Fig. 13 shows the changes of $I_{\rm rms}$, output torque, and speed of the machine when the proposed strategy is changed to the traditional strategy. Before 28 s, the machine works under the harmonic injection control strategy and has entered a stable state. At this point, $I_{\rm rms}$ is 19.3 A, load torque is 2.76 N·m, and the speed is 1500 r/min. Switching to the conventional strategy at 28 s, while keeping the speed at 1500 r/min and the load torque at 2.76 N·m. After the machine enters steady state, $I_{\rm rms}$ increases to 20.4 A. When the speed and load torque remain unchanged, $I_{\rm rms}$ with the proposed strategy is lower than that of the conventional control strategy, indicating that the proposed strategy can improve the output torque of the dc-biased-VRM while $I_{\rm rms}$ remains unchanged.

To test the dynamic performance of the proposed strategy, the acceleration and load variation experiments were carried out. In Fig. 14(a), the load is changed from 0.72 to 2.75 N·m at 1500 r/min. The results show that the speed drops temporarily when the load changes but can soon be adjusted to the reference value. The current overshoot of the q-axis and 0-axis is also relatively small, indicating that the method has a strong anti-interference ability while accurately controlling the current. In Fig. 14(b), the load is 2.75 N·m and the machine speed gradually increases from 1000 to 1500 r/min. This strategy can accurately track the reference speed and has good dynamic response ability, which is advantages from the use of ANF to detect the current deviation dynamically.

With the increase of the machine speed, the frequency of the second harmonic that needs to be injected will also increase, which puts forward strict requirements on the performance of the control strategy. The harmonic current orthogonal component distribution strategy proposed in this article gives the static reference value of harmonic current, and the harmonic current can be adjusted effectively by using PI regulator. In addition, the PI regulator's output voltage signal is compensated with advance phase angle strategy, which further improves the stability of the control system. Therefore, the proposed second harmonic injection strategy can improve the output torque in a wide speed range, and further improve the efficiency of the machine. To verify this conclusion, the $I_{\rm rms}$ is set to 19 A when the speed is below 1500 r/min. When the speed is higher than 1500 r/min, the output power of the machine is fixed at 429 W. The experiment

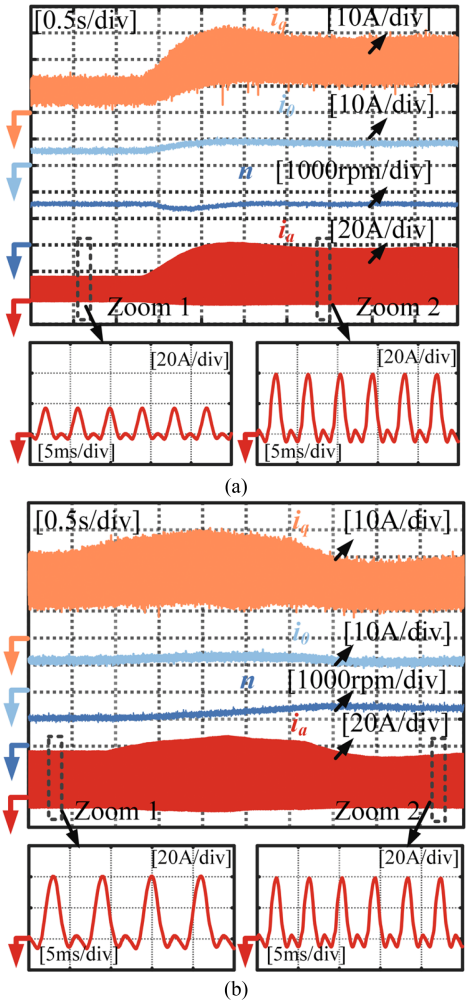

Fig. 14. Experimental results of dynamic performance of proposed strategy. (a) Load variation. (b) Machine acceleration.

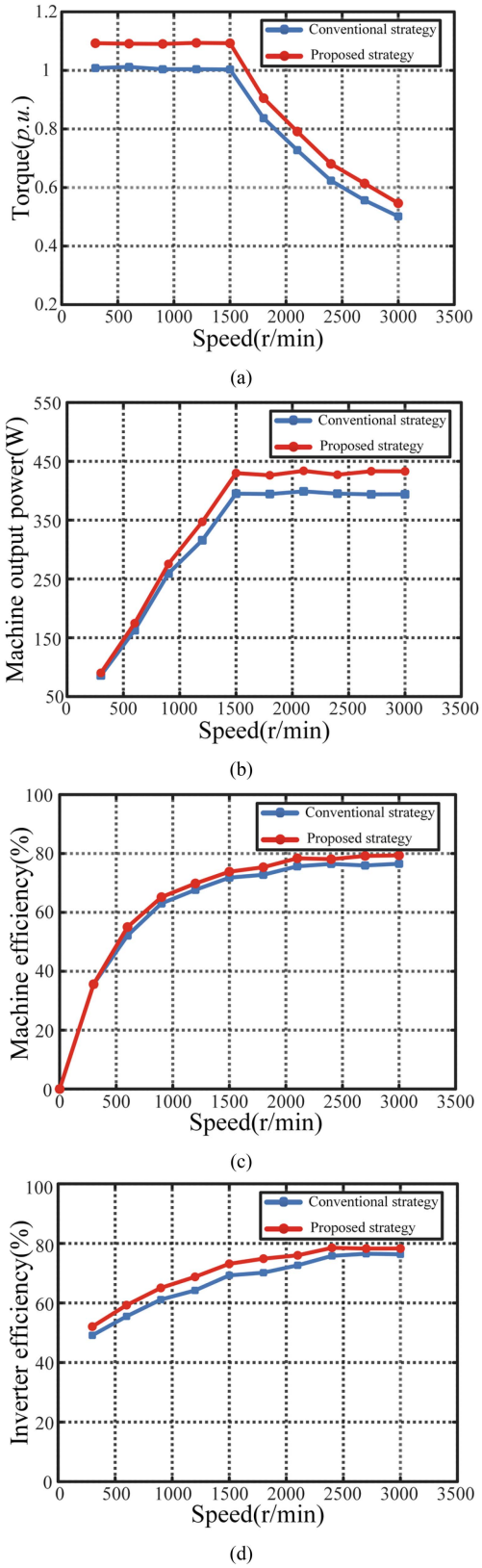

Fig. 15. Experimental results of the proposed and conventional strategies. (a) Torque. (b) Machine output power. (c) Machine efficiency. (d) Inverter efficiency.

was repeated by changing the speed and recording the corresponding output torque. In Fig. 15(a), when the machine speed is 1500 r/min and I_{rms} is 19 A, the per unit value of the machine output torque is 1 using the conventional control strategy, and the results show that when the machine speed is below 3000 r/min, the output torque is increased by 8.76%, which indicates that the proposed strategy has a good output torque improvement effect in a wide speed range.

Due to the existence of second harmonic current, the energy loss of the machine is slightly increased, but because of the improvement of current utilization, the output power of the machine is greatly improved, as shown in Fig. 15(b), so in Fig. 15(c), the overall efficiency of the machine is improved. In addition, the efficiency of the inverter is further improved in Fig. 15(d), this is because under the same experimental conditions, the input power of the inverter is increased and the proportion of energy loss in the total energy is reduced by using the strategy proposed in this article.

VI. Conclusion

This article presents an improved harmonic current injection control strategy dc-biased-VRM based on current orthogonal component distribution to enhance output torque. A novel distribution method of harmonic current orthogonal component is proposed in the synchronous rotating coordinate system to provide reference value of harmonic current injection, then the feedback harmonic components of phase current are quickly extracted by ANF and finally adjusted by PI regulator. Furthermore, in order to accurately track the harmonic reference value, a tracking strategy of harmonic current orthogonal component with advance angle compensation is proposed, which realizes the complete compensation of harmonic voltage. Besides, the angle error of harmonic current injection is reduced, and the stability of the control system is improved. Finally, the accurate injection of amplitude and angle of harmonic current is realized.

The experimental results demonstrate the superiority of the proposed harmonic current injection control strategy. Compared with the conventional control strategy, this proposed method can accurately inject the second harmonic current into the stator winding, and can increase the output torque of dc-biased-VRM by 8.76%, further improving the current utilization rate and output efficiency.

References

[1] Z. Q. Zhu, X. Liu, and Z. Pan, "Analytical model for predicting maximum reduction levels of vibration and noise in switched reluctance machine by active vibration cancellation," *IEEE Trans. Energy Convers.*, vol. 26, no. 1, pp. 36–45, Mar. 2011.

[2] S. Jia, R. Qu, W. Kong, D. Li, and J. Li, "Flux modulation principles of DC-biased sinusoidal current Vernier reluctance machines," *IEEE Trans. Ind. Appl.*, vol. 54, no. 4, pp. 3187–3196, Jul./Aug. 2018.

[3] S. Jia, R. Qu, W. Kong, D. Li, J. Li, and R. Zhang, "Stator/rotor slot and winding pole pair combinations of DC-biased current Vernier reluctance machines," *IEEE Trans. Ind. Appl.*, vol. 54, no. 6, pp. 5967–5977, Nov./Dec. 2018.

[4] Z. Yu, W. Kong, C. Gan, and R. Qu, "Power converter topologies and control strategies for DC-biased Vernier reluctance machines," *IEEE Trans. Ind. Electron.*, vol. 67, no. 6, pp. 4350–4359, Jun. 2020.

[5] Z. Chen, W. Kong, Z. Li, J. Hao, and R. Qu, "Novel harmonic current controller for DC-biased Vernier reluctance machines based on virtual winding," *IEEE Trans. Ind. Electron.*, vol. 70, no. 9, pp. 8788–8799, Sep. 2023.

[6] Z. Yu et al., "Optimal three-dimensional current computation flux weakening control strategy for DC-biased Vernier reluctance machines considering inductance nonlinearity," *IEEE Trans. Power Electron.*, vol. 34, no. 2, pp. 1560–1571, Feb. 2019.

[7] Z. Yu, W. Kong, D. Li, R. Qu, and C. Gan, "Power factor analysis and maximum power factor control strategy for six-phase DC-biased Vernier reluctance machines," *IEEE Trans. Ind. Appl.*, vol. 55, no. 5, pp. 4643–4652, Sep./Oct. 2019.

[8] Z. Yu, W. Kong, and R. Qu, "Direct torque control strategy for DC-biased Vernier reluctance machines capable of zero-sequence current regulation," *IEEE Trans. Ind. Electron.*, vol. 68, no. 3, pp. 2024–2033, Mar. 2021.

[9] Z. Yu et al., "Fault-tolerant control strategy of the open-winding inverter for DC-biased Vernier reluctance machines," *IEEE Trans. Power Electron.*, vol. 34, no. 2, pp. 1658–1671, Feb. 2019.

[10] Y. Li, H. Yang, and H. Lin, "Investigation of torque improvement mechanism in emerging switched flux PM machines," *IEEE J. Emerg. Sel. Topics Power Electron.*, vol. 10, no. 2, pp. 1860–1869, Apr. 2022.

[11] W. Ding, H. Bian, K. Song, Y. Li, and K. Li, "Enhancement of a 12/4 hybrid-excitation switched reluctance machine with both segmented-stator and -rotor," *IEEE Trans. Ind. Electron.*, vol. 68, no. 10, pp. 9229–9241, Oct. 2021.

[12] E. F. Farahani, M. A. J. Kondelaji, and M. Mirsalim, "An innovative hybrid-excited multi-tooth switched reluctance motor for torque enhancement," *IEEE Trans. Ind. Electron.*, vol. 68, no. 2, pp. 982–992, Feb. 2021.

[13] G. J. Li, K. Zhang, Z. Q. Zhu, and G. W. Jewell, "Comparative studies of torque performance improvement for different doubly salient synchronous reluctance machines by current harmonic injection," *IEEE Trans. Energy Convers.*, vol. 34, no. 2, pp. 1094–1104, Jun. 2019.

[14] Z. Q. Zhu, B. Lee, L. Huang, and W. Chu, "Contribution of current harmonics to average torque and torque ripple in switched reluctance machines," *IEEE Trans. Magn.*, vol. 53, no. 3, Mar. 2017, Art. no. 8100909.

[15] Z. Yu, W. Kong, R. Qu, Z. Li, and D. Li, "Dual-inverter PWM scheme for DC-biased Vernier reluctance machines with reduced switching frequency capable of zero-sequence current regulation," *IEEE Trans. Ind. Electron.*, vol. 69, no. 2, pp. 1276–1287, Feb. 2022.

[16] G. Liu, Z. Lin, W. Zhao, Q. Chen, and G. Xu, "Third harmonic current injection in fault-tolerant five-phase permanent-magnet motor drive," *IEEE Trans. Power Electron.*, vol. 33, no. 8, pp. 6970–6979, Aug. 2018.

[17] L. Wu and Z. Lyu, "Harmonic injection-based torque ripple reduction of PMSM with improved DC-link voltage utilization," *IEEE Trans. Power Electron.*, vol. 38, no. 7, pp. 7976–7981, Jul. 2023.

[18] B. Lee, Z. Q. Zhu, and L. R. Huang, "Torque ripple reduction for 6-stator/4-rotor-pole variable flux reluctance machines by using harmonic field current injection," *IEEE Trans. Ind. Appl.*, vol. 53, no. 4, pp. 3730–3737, Jul./Aug. 2017.

[19] G. Yang, H. Hussain, S. Li, J. Zhang, and J. Yang, "Fault-tolerant control for multiphase induction machines with torque ripple reduction considering harmonic injection," *IEEE Trans. Power Electron.*, vol. 37, no. 12, pp. 14005–14010, Dec. 2022.

[20] T. Wang, L. Guo, K. Wang, J. Wu, C. Liu, and Z. Zhu, "Generalized predictive current control for dual-three-phase PMSM to achieve torque enhancement through harmonic injection," *IEEE Trans. Power Electron.*, vol. 38, no. 5, pp. 6422–6433, May 2023.

[21] S. Somkun, S. Srita, T. Kaewchum, A. Pannawan, C. Saeseiw, and P. Pachanapan, "Adaptive notch filters for bus voltage control and capacitance degradation prognostic of single-phase grid-connected inverter," *IEEE Trans. Ind. Electron.*, vol. 70, no. 12, pp. 12190–12200, Dec. 2023.

[22] J. Man, L. Chen, V. Terzija, and X. Xie, "Mitigating high-frequency resonance in MMC-HVDC systems using adaptive notch filters," *IEEE Trans. Power Syst.*, vol. 37, no. 3, pp. 2086–2096, May 2022.

[23] Z. Li, Z. Yu, W. Kong, R. Qu, and D. Li, "An accurate harmonic current suppression strategy for DC-biased Vernier reluctance machines based on adaptive notch filter," *IEEE Trans. Ind. Electron.*, vol. 69, no. 5, pp. 4555–4565, May 2022.

[24] Y. Fan, Q. Zhang, W. Wang, and X. Zhou, "Speed regulation system of a flux-modulated permanent-magnet in-wheel motor based on sliding mode control and adaptive notch filter," *IEEE Trans. Energy Convers.*, vol. 33, no. 4, pp. 2183–2190, Dec. 2018.

Xiang Zhang was born in Pingdingshan, China. He received the B.E.E. degree in electrical engineering and automation from Yangzhou University, Yangzhou, China, in 2022. Since 2022, he has been working toward the M.S. degree in control engineering with the School of Electrical Engineering and Automation, Hefei University of Technology, Hefei, China.

His research interests include control strategy of reluctance machines.

Jiwen Zhao (Senior Member, IEEE) was born in Dangshan, China. He received the Ph.D. degree in precision instruments and machinery from the University of Science and Technology of China, Hefei, China, in 2005.

Since 2019, he has been working with the School of Electrical and Automation Engineering, Hefei University of Technology, Hefei, China. He is currently a Professor with the School of Electrical and Automation Engineering, Hefei University of Technology, Hefei, China. His research interests include linear machine optimization design, linear machine control and photoelectric detection technology.

Zixiang Yu (Member, IEEE) was born in Liaoning, China, in 1993. He received the B.E.E. degree in electrical engineering, from Dalian Maritime University, Dalian, China, in 2015, and the M.S. and Ph.D. degrees in electrical engineering from Huazhong University of Science &Technology, Wuhan, China, in 2018 and 2021, respectively.

Since 2021, he has been an Associate Professor in electrical engineering with the School of Electrical Engineering and Automation, Hefei University of Technology, Hefei, China. His current research focuses on control strategy of PM machines, reluctance machines, and multiphase machines.

Zhenbao Pan (Member, IEEE) was born in Guilin, China. He received the B.S. degree in electrical engineering and automation from Anhui University, Hefei, China, in 2014, the M.S. degree in detection technology and automatic equipment from Anhui University, Hefei, China, in 2017, and the Ph.D. degree in electrical engineering from Southeast University, Nanjing, China, in 2022.

Since 2022, he has been with Hefei University of Technology, where he is currently a Lecturer with the School of Electrical Engineering and Automation. His main research interests include design, analysis, optimization and control of permanent-magnet machines with particular reference to linear machines and arc machines.